Audio Engineering Society
Convention Paper

Presented at the 133rd Convention
2012 October 26–29 San Francisco, CA, USA



# Study of the interaction between radiating systems in a coaxial loudspeaker

Espí, A.[1], Cárdenas, W.A.[2], Martínez, J. [1], Ramis, J.[2], Carbajo, J.[2]

[1] Acústica Beyma, S.L., Moncada, Valencia, 46113, Spain

alejandro.espi@beyma.com, j.martinez@beyma.com

[2] IUFACT, Universidad de Alicante, 03080, Spain

wacp1@alu.ua.es, jramis@ua.es, jesus.carbajo@ua.es

## ABSTRACT

In this work, the procedure followed to study the interaction between the mid and high frequency radiating systems of a coaxial loudspeaker is explained. For this purpose, a numerical Finite Element model was implemented. In order to fit the model, an experimental prototype was built and a set of experimental measurements, electrical impedance and pressure frequency response in an anechoic plane wave tube among these, were carried out. So as to take into account the displacement dependent nonlinearities, a different input voltage parametric analysis was performed and internal acoustic impedance was computed numerically in the frequency domain for specific phase plug geometries. Through inversely transforming to a time differential equation scheme, a lumped element equivalent circuit to evaluate the mutual acoustic load effect present in this type of acoustic coupled systems was obtained. Additionally, the crossover frequency range was analyzed using the Near Field Acoustic Holography technique.

## 1. INTRODUCTION

In this work, the procedure followed to study the interaction between the mid and high frequency radiating systems of a coaxial loudspeaker is explained. The mutual acoustic load was studied based on a lumped parameter nonlinear model that takes into account the effect that the adiabatic process in the compression chamber causes over the diaphragms ([1] and [2]), as well as the mechanical and electrical nonlinearities on the stiffness of the suspension, the force factor and the voice coil inductance. For this purpose, a numerical Finite Element model was implemented.

In order to fit the model, an experimental prototype was built, consisting of a 6 inches annular midrange

loudspeaker and a 2 inches tweeter attached to a folded duct. This system is acoustically loaded with a phase plug in the case of the midrange speaker and a bullet piece which in turn forms the inner part of the folded duct. The initial numerical model parameters were fitted from electrical impedance and pressure frequency response measurements in the small signal regime. So as to determine the independent components (compression chambers, propagation paths, geometry) effect on the whole system operation, each loudspeaker was measured separately in an anechoic plane wave tube. Also, and so as to identify the contribution of the main vibration modes of the diaphragms, a numerical modal analysis was carried out, using the Young modulus and loss factor data of the membrane and suspension material provided experimentally by applying direct and inverse techniques.

Once the linear model was properly fitted, a different input voltage parametric analysis was performed, making it possible to establish the large signal regime behavior of both transducers (midrange and tweeter). Since a lumped parameter model does not contemplate specific geometries, the acoustic radiation impedance presented by each phase plug was calculated numerically and inversely transformed to the time domain. Based on the numerical solution of time domain differential equations, the dynamical behavior of the diaphragms and the nonlinear air compression in the compression chambers were obtained.

The superposition of the response of each loudspeaker was compared with that measured experimentally to establish the effect of the mutual coupling acoustic load and to evaluate the distortion generated for various input voltage levels. Furthermore, the crossover frequency range of the whole radiating system was analyzed using the Near Field Acoustic Holography (NAH) technique, widely used in the characterization and assessment of loudspeakers performance.

The structure of the paper is as follows; in section 2 the basic concepts that support the lumped parameter and describe the behavior of the speaker model are briefly explained, with special emphasis on nonlinear contributions. In section 3, the approach used to address each of the problems that arise are explained, specifically, the results of experimental measurements are explained and discussed. We present the FEM numerical model implemented to calculate the acoustic impedance loads on each of the speakers, which are determined by the specific geometry of the phase plug and horn. The block diagram of the application implemented to solve the set of differential equations in time domain is also presented. In Section 4, the results that validate the model and the system response are studied, as well as the effect of different changes in both geometries, with special emphasis on the transition zone between both radiating systems. The effect of an increase of the input voltage in the non-linear response (THD %) is also investigated. In order to study the radiation of coaxial speaker in the crossover region, some results of the Near-Field Acoustic Holography (NAH) measurements are presented. Finally, section 5 describes the main conclusions of this work.

## 2. CONCEPTS

Different methods based on the principles of electrodynamic loudspeaker have been developed to model horn drivers and compression drivers, added the effects due to air layers formed in the compression chambers and phase plugs, as well as the nonlinear propagation inside the phase plug and the complex impedance of the horn ([1], [2], [3] and [4]). The method used to develop the present study is based on the numerical solution of a set of differential equations that describe the response of the loudspeaker to any stimulus like noise, sine-sweeps or music.

As is well known, the loudspeaker is a nonlinear system, where its major nonlinearities depend on the voice coil displacement and current ([5] and [6]).

The electro mechanic mechanism of a loudspeaker can be divided in two parts: electrical and mechanical, both of them coupled by the force factor $Bl(x)$. The differential equations which describe the electrical part are:

$$u(t) = i(t)R_e + \frac{d(L_e(x)i(t))}{dt} + \frac{d(L_2(x)i_2(t))}{dt} + Bl(x)\frac{dx}{dt} \qquad (1)$$

$$\frac{d(L_2(x)i_2(t))}{dt} = (i(t) - i_2(t))R_2(x) \qquad (2)$$

where $u(t)$ is the input voltage and $i(t)$ is the current in the voice coil, both of them are time dependent, $R_e$ is the dc resistance of the voice coil, $L_e(x)$ is the voice coil inductance and depends on the voice coil displacement $x$; $L_2(x)$, $i_2(t)$ and $R_2(x)$ describe the eddy currents

at high frequencies, based on the LR-2 model discussed in [7], and $Bl(x)$ is the force factor.

Regarding the mechanical part, a nonlinear term in the compliance associated to the compression chamber coupled to the phase plug and the rear chamber must be previously explained. As it is known, one of the components that add distortion to the acoustic output is the nonlinear relationship of the pressure and volume changes in these two chambers. This relationship can be expressed by the adiabatic equation as:

$$P_0 V_0^{\gamma} = (P_0 + p)(V_0 - V)^{\gamma} \tag{3}$$

where $p$ is the acoustic pressure in the chamber, $V_0$ the chamber volume, $P_0$ the atmospheric pressure, $\gamma$ adiabatic constant (in air, $\gamma \approx 1.4$) and $V$ represents the instantaneous variation of the chamber volume, that depends on the diaphragm displacement, being $V = S_d x$, where $S_d$ and $x$ are the surface and diaphragm displacement respectively.

Given that the compression chamber of a driver is not a completely closed enclosure and that is connected with the outside region through the holes in the phase plug and throat of the horn, in [1] is shown that:

$$p(x, x_p) = P_0 \left[ \left( 1 - \frac{S_d x - S_p x_p}{V_0} \right)^{-\gamma} - 1 \right] \tag{4}$$

To study the behavior of the compression driver, equation (4) should be combined with the differential equations system that balances forces and voltages that govern the diaphragm movement. The Taylor expansion of (4) can be transformed into differential equation if the input impedance of the phase plug and horn is assumed to be the acoustic impedance $\rho_0 c$ of a plane wave that propagates in air, being $\rho_0$ the density and $c$ velocity of sound in air respectively. Given that this hypothesis is not applicable in our case, is necessary to use a set of equations capable of taking into account the complex acoustic load of the phase plug and the specific horn.

According to Voishvillo in [1], the acoustic impedance load of the phase plug and horn can be approximated by a fractional-rational function as:

$$Z(s) = \frac{p(s)}{v_p(s)} = \rho_0 c \prod_{i=1}^{n} \frac{s^2 + b_{1i} s + b_{0i}}{s^2 + a_{1i} s + a_{0i}} \tag{5}$$

being $p(s)$ the chamber sound pressure and $v_p(s)$ the velocity of the air in the phase plug, both expressed in the Laplace domain, and $b_{1i}$, $b_{0i}$, $a_{1i}$ and $a_{0i}$ the function coefficients. By performing an inverse transform is possible to convert the acoustic impedance in a differential operator and to obtain a set of differential equations that takes into account the complex impedance of the phase plug and horn.

The displacement in the phase plug $x_p$ can be expressed in terms of the pressure in the chambers as:

$$\frac{d^n x_p}{dt^n} = \frac{1}{\rho c}\left( \frac{d^{n-1} p}{dt^{n-1}} + \frac{d^{n-2} p}{dt^{n-2}} g_{n-2} + \frac{dp}{dt} g_1 + p g_0 \right) - \frac{d^{n-1} x_p}{dt^{n-1}} h_{n-1} - \frac{d^{n-2} x_p}{dt^{n-2}} h_{n-2} \ldots - \frac{dx_p}{dt} h_1 \tag{6}$$

where $g_i$ and $h_i$ are the adjustment coefficients. If $x_p$ and $x$ are substituted in equation (4) and after the pressure in the compression chamber and its derivatives are replaced in equation (6), this expression can be *n-times* integrated numerically to obtain $x_p$.

In this work, the acoustic impedance is approximated by the transfer function:

$$Z(s) = \rho c \frac{s^2 + b_1 s + b_0}{s^2 + a_1 s + a_0} \tag{7}$$

where $b_1$, $b_0$, $a_1$ and $a_0$ are the adjustment coefficients needed to approximate this transfer function to that obtained numerically using finite element. Then equation (6) can be rewritten as:

$$\frac{d^3 x_p}{dt^3} = \frac{1}{\rho c}\left( \frac{d^2 p}{dt^2} + a_1 \frac{dp}{dt} + a_0 p \right) - b_1 \frac{d^2 x_p}{dt^2} - b_0 \frac{dx_p}{dt} \tag{8}$$

In this case, the derivatives of the pressure in the compression chamber are obtained analytically.

Regarding the mechanical description of the loudspeaker displacement, the force equilibrium

equation [3] is presented adding an additional term $pS_d$ that describes the compression chamber response to the diaphragm movement:

$$\begin{aligned} & Bl(x)i(t) - F_m(x,i,i_2) = m_{ms}\frac{d^2x}{dt^2} + \\ & + \left[ R_{ms} + R_{mv}(x) + R_p\frac{dx_p}{dt} \right]\frac{dx}{dt} + \\ & + \left[ K_{ms}(x) + K_r(x) \right]x(t) + pS_d \end{aligned} \tag{9}$$

where $R_{ms}$ is the system mechanical resistance, $R_{mv}(x)$ refers to the thermo viscous losses present in the compression driver and $R_p$ stands for the losses caused by the turbulences in the phase plug, while $K_{ms}(x)$ and $K_r(x)$ correspond to the suspension and rear chamber stiffness respectively. The reluctance force $F_m(x,i,i_2)$ can be modeled in an approximated manner as:

$$F_m(x,i,i_2) = \frac{-i^2(t)}{2}\frac{dL_e(x)}{dx} - \frac{-i_2^2(t)}{2}\frac{dL_2(x)}{dx} \tag{10}$$

This nonlinear differential equation system is solved using a Runge-Kutta algorithm in a block oriented implementation as will be shown in section 3.3.

## 3. APPROACH

This section describes the specific approach used to address each of the key points of the process. The first step was to perform some measurements on a prototype built for this purpose. Then, the basic data is supplied to the FEM model implemented to obtain the acoustic impedance, and finally the block diagram of the application developed to solve the differential equations is presented.

### 3.1. Experimental measurements

Figure 1 shows a picture and a cross-sectional view of the prototype built used to calibrate the model.

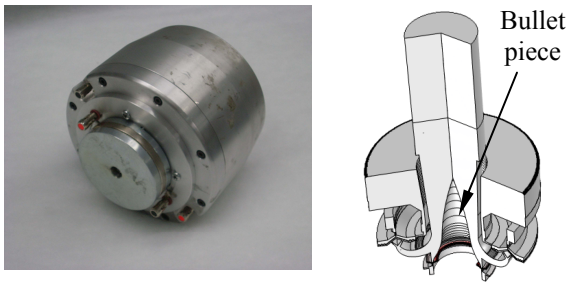


Figure 1: Prototype built: (a) picture and (b) cross-sectional view.

For this purpose, sound pressure measurements were preformed in a plane wave tube with anechoic termination as that shown in Figure 2.

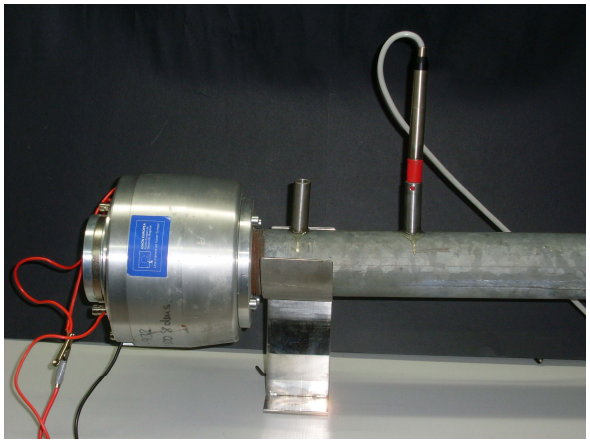

Figure 2: Plane wave tube with driver.

To identify and characterize the frequency range over which the Tweeter (TWT) has an important influence, some measurements of the frequency response were carried out. In a first step, the polarity of the exciting signal of the tweeter was inverted. Figure 3 shows the effect of this polarity inversion in the coaxial loudspeaker. As it can be seen, the cancellation effect is more evident for frequencies located in a very wide range (between 3 kHz and 7 kHz), where variations reach levels of over 7 dB, as in the case of 6 kHz. The area between 7 kHz and 9 kHz presents a dip of more than 10 dB with respect to the adjacent bands for both cases even though is not in the transition zone of the speakers.

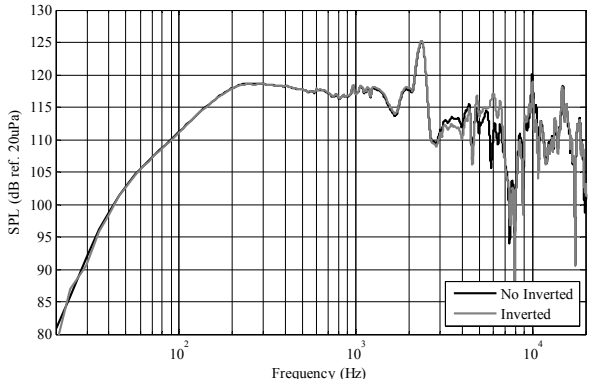


Figure 3: Effect of the phase inversion in the coaxial speaker SPL.

In a second step and so as to analyze the interaction between common cavities involved in the acoustic paths of the system, the folded duct section corresponding to the midrange speaker was covered with plastic mass reducing the acoustic load volume of the tweeter diaphragm. Figure 4 shows a comparison between the tweeter frequency response for the normal configuration and the modified one.

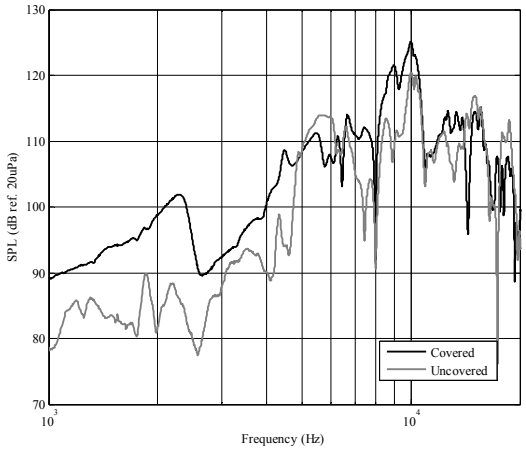


Figure 4: Effect of the acoustic paths modification in the tweeter SPL.

By means of an analysis of Figure 4, an increase of the SPL due to the reinforcement of the acoustic energy propagation through an only path is evidenced, but it can be also appreciated that some of the resonance frequencies associated to the covered cavity are attenuated, as in the case of 6 kHz. These and other effects can be studied with the model implemented in this work, since it can take into account changes in the geometry and the acoustic impedance load of the speakers, being of great interest in the design process of these type of speakers.

### 3.2. Computation of the acoustic impedance with Finite Element Analysis

One way to integrate into the analysis of the speaker performance some factors like the complex geometries of the phase plug and ducts on which the speakers radiate, is to numerically calculate the acoustic impedance load of each diaphragm. This numerical experiment is performed in harmonic regime using the Finite Element Method.

The axisymmetric model developed consists of 21428 triangular elements for a discretized cross section of 6961 $mm^2$ comprising compression chambers, rear chambers and a folded duct considered a mutual load for both diaphragms. Figure 5 shows the results of the numerical model at 13 kHz, where the radiation boundary conditions and PML region are properly depicted.

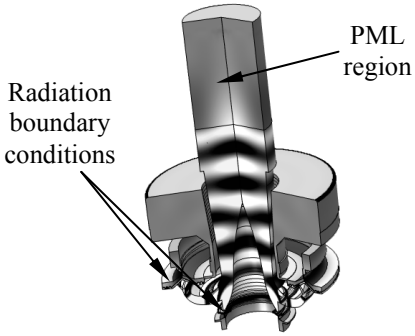


Figure 5: Details of the axisymmetric numerical model harmonic analysis results at 13 kHz.

Once the acoustic impedance is calculated, the transfer function $Z(s)$ used in the differential equations model is adjusted.

Figure 6 shows the acoustic impedances in the case of the Midrange speaker and the Tweeter in a first approximation, where the acoustic impedance is computed as the ratio of the averaged pressures and particle velocities in the proximities of the diaphragm. It

must be empathized that the acoustic impedance value presents important deviations depending on the position considered for the calculations.

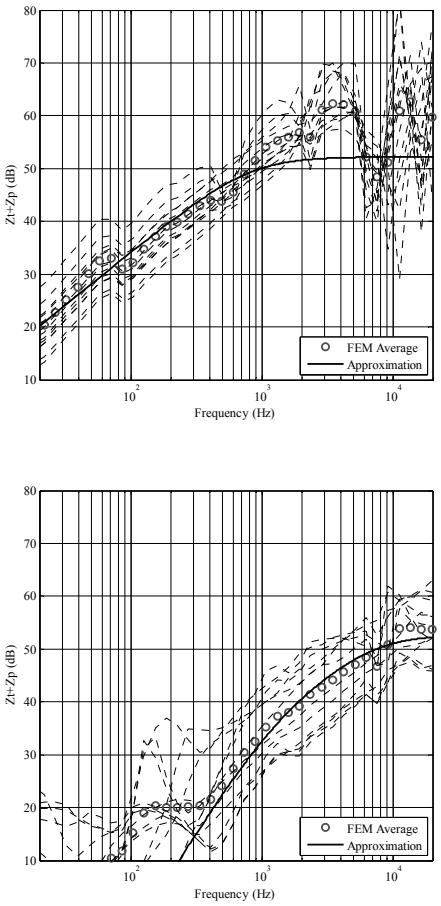


Figure 6: Acoustic impedances for the Midrange speaker (up) and the Tweeter (down) computed and fitted with $a_0$ , $a_1$ , $b_0$ and $b_1$ coefficients.

It should be noted that variations in the impedance for the numerical calculation involve more than a single resonance along the frequency range, which cannot be adjusted with great accuracy by these coefficients. To achieve a behavior of this type is necessary to handle a transfer function of higher order, imposing derivatives of third or fourth order in the differential equations system development.

### 3.3. Block-Oriented system for solving the Differential Equations

The block diagram used to solve the nonlinear differential equations system in the time domain is shown in Figure 7, where acoustic, mechanical and electrical parts as well as the variables that relate them, are shown.

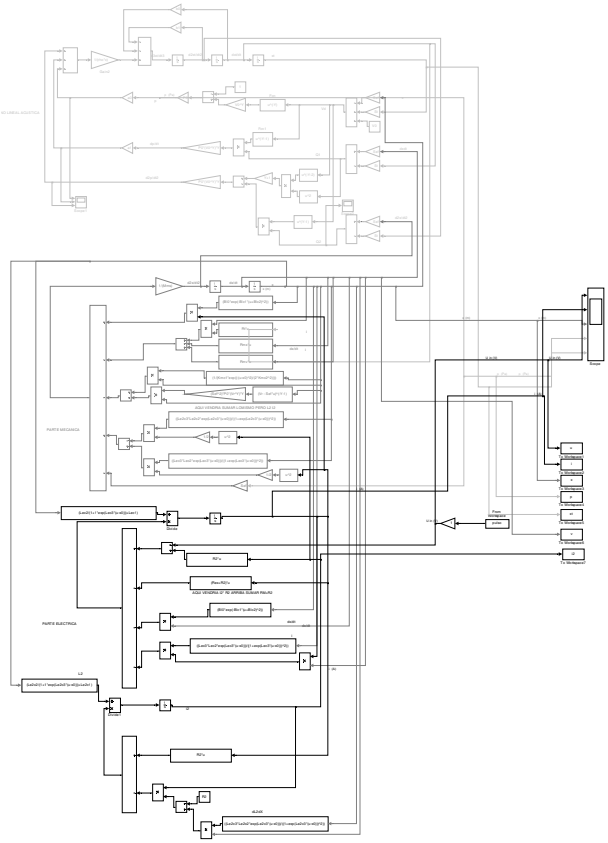

Figure 7: Block-diagram used to solve the nonlinear differential equations system (gray: acoustical, dark-gray: mechanical and black: electrical)

### 3.4. Swept-Sine based linear and nonlinear analysis

In order to study the distortion behavior of the compression driver, a widely used non-linear systems characterization methodology based in Exponential Sweep Method was employed. This is accomplished by generating a signal that varies in frequency over time. As expected, with this type of stimulus it can be only

studied the harmonic distortion. The input signal is defined as:

$$x(t) = \sin\left[\omega_1 \frac{T}{c}\left(e^{t\frac{c}{T}} - 1\right)\right] \quad (11)$$

where $t \in [0,T]$ is the time interval, $T$ is the signal duration and $c = \ln(\omega_2 / \omega_1)$, with $\omega_1$ and $\omega_2$ the sine swept start frequency and final frequency respectively. A weakly nonlinear system excited by this signal produces a response signal $y(t)$ with higher order harmonics.

In order to complete the system identification, the output signal $y(t)$ is convolved with an inverse sweep $x'(t)$ which satisfies $x(t) * x'(t) = \delta(t)$, obtaining:

$$s(t) = y(t) * x'(t) \quad (12)$$

The inverse sweep compensates for the group delay and the stimulus magnitude spectrum, and can be obtained from the input signal applying the Fourier transform [8]:

$$X'(\omega) = \frac{X'(-\omega)}{|X(\omega)^2|} \quad (13)$$

where $X(\omega)$ is the complex spectrum of the input signal $x(t)$ and $X'(\omega)$ the spectrum of the inverse sweep $x'(t)$.

### 3.5. Radiation study by means of NAH

The Near-Field Acoustic Holography (NAH) technique is a procedure used to reconstruct the sound field and the vibration velocity of an object or sound source from measurements with microphones in a plane parallel and close to the source (hologram plane). This technique had its origin in a work by Williams and Maynard in 1985 ([9] and [10]), that improved conventional holography by near-field measurements, which allow to cover a wide frequency range and also to capture the evanescent waves (subsonic waves that decay exponentially with distance from the source [11]) created by the sound source and that contain high resolution information about the source ([12]). In the present work, the measurement grid used had a spatial resolution of 4 mm in a parallel plane placed 5 mm in front of the compression driver output.

Figure 8 shows the experimental setup used for the NAH measurements.

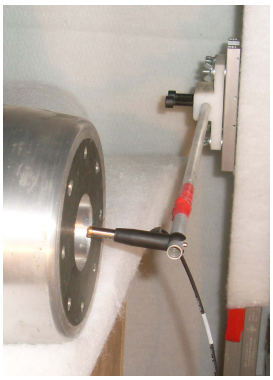

Figure 8: Experimental setup used for the NAH measurements.

## 4. RESULTS

### 4.1. Validation of the model

This section explains in detail the process undertaken to determine the main features of the model. Figure 9 shows the curves of measured and simulated pressure of both speakers for an input signal of 720 mV.

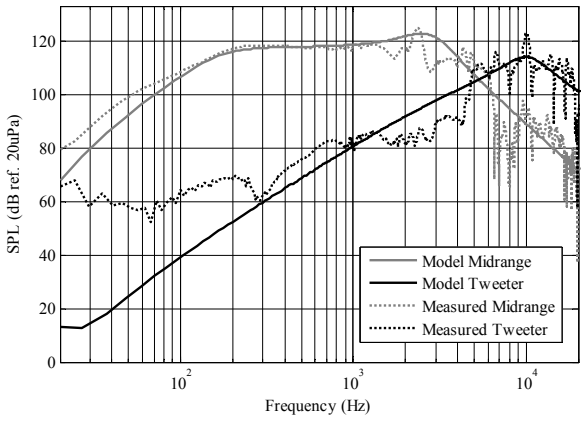


Figure 9: Measured and simulated SPL frequency response of the coaxial loudspeaker.

Note that the model takes into account the most representative characteristics of the real driver units. For this reason, some of the aspects related to the membrane structural behavior cannot be properly modeled.

The global system response is presented in Figure 10. It can be appreciated a slight good agreement between computed and measured data in the acoustic crossover region.

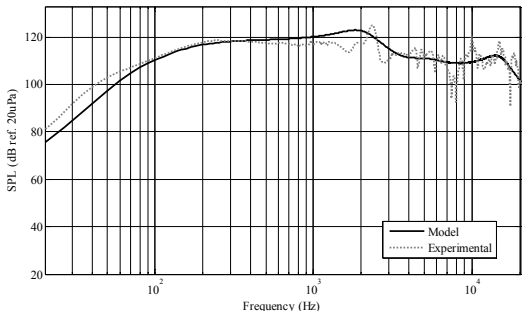


Figure 10: Comparison between computed and measured SPL.

### 4.2. Assessment of the system behavior in the transition band

A first approach to the problem would conclude that the transition zone of the speakers is controlled by mechanical parameters such as the moving mass of the tweeter, the compliance of the suspension and some other geometrical factors as the air volumes cavities and surfaces of the ducts attached to the vibration of the half-inch speaker.

The high frequency region is more affected by the geometry that forms the bullet piece with the folded duct. The effect of phase inversion of the system, discussed in section 3.1 (Figure 3), allows to determine the spectral regions that are more affected by the destructive interference within this folded duct. This information is useful as an initial criterion of optimization of the radiating system and an alternative that can improve the frequency response in regions above the transition zone, controlled by the high frequency transducer.

In a first approximation, the solution to this problem could be to increase the volume of the compression chamber to avoid the roll-off in the high frequency range to be so abrupt or to modify the tweeter so that the resonance frequency decreases to the pass band immediately next to the Midrange decay. Although both possibilities are feasible, the design of a system of this type involves a compromise between efficiency and "flatness-smoothness" of the acoustic response.
To study this phenomenon without the need to physically modify the prototype, different simulations of the model implemented are performed for different values of mass $m_{ms}$ and volume of the compression chamber $V_0$, which add rigidity to the system changing the resonance frequency of the tweeter. Figures 11 and 12 show the results of the simulations for different values of mass and volume, where discontinuous lines represent the Tweeter and Midrange loudspeakers individual responses respectively.

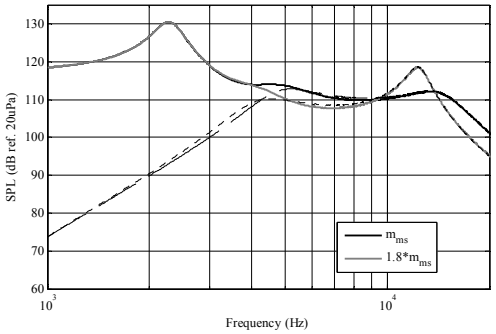


Figure 11: Effect in the overall response of the modification of the $m_{ms}$ of the tweeter.

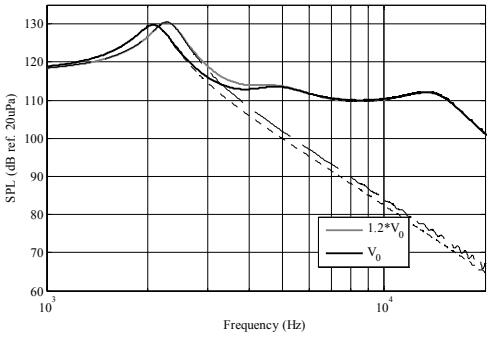


Figure 12: Effect in the transition zone of the variation of the $V_0$ of the compression chamber.

An increase of the moving mass of the tweeter implies a decrease of the resonance frequency that makes the pass band to be positioned nearer to the decay of the Midrange and thereby to achieve a higher gain when it is almost duplicated. In the other hand, an increase of the volume of the compression chamber makes the response curve to be shifted to higher frequencies.

### 4.3. THD (%)

In this section, an analysis of harmonic distortion generated by the speaker is carried out from an experimental and simulation approach. Since the model is based on the numerical solution of a set of differential equations in the time domain, the excitation signal can be any time sequence sampled at the same rate as the time step of the algorithm. In this case the input signal is generated with a sampling rate of 882 kHz, due to the temporal resolution required to fix the model. Once the signals for the state variables such as pressure, velocity and displacement currents are obtained, a decimation process is performed so as to work at the same sampling rate that in the experimental measurements.

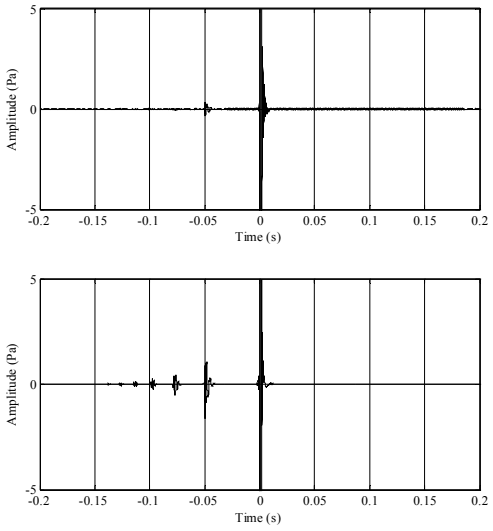


Figure 15: Model linear response and higher order harmonics for two different input voltages: 800 mV (up) and 1900 mV (down).

The swept sine used has a length of 0.5 s and covers a frequency range from 20 Hz to 20 kHz. Figure 15 shows the output signal convolved with the inverse sweep for input voltages of 800 mV and 1900 mV. It must be remarked that an increment of this input voltage involves the higher order harmonics appearance due to the nonlinear distortion imposed by the electrical and mechanical parameters as well as the adiabatic compression in the compression and rear chambers.

In Figure 16, frequency response (FR) and harmonic distortions are shown for two input voltages. It can be appreciated that the measured harmonic distortion is more pronounced for the 3$^{th}$ order harmonic (H3) than for the 2$^{nd}$ order harmonic (H2) when the input voltage is increased from 800 mV to 1900 mV.

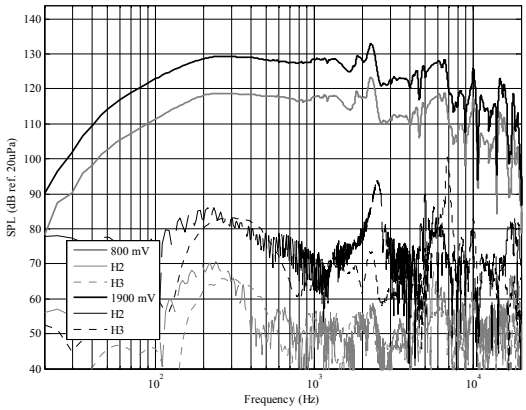


Figure 16: Measured harmonic distortion increment for two input voltages: 800 mV and 1900 mV.

### 4.4. NAH results

As it was discussed in section 3.1, the geometrical shape of the bullet piece and the folded duct can be optimized so as to improve the system performance in the high frequency range. The NAH technique allows to study in detail the effects on the system response of changing these geometries.

Figure 17 shows the sound pressure in a plane of 100x100 mm close to the driver output for different frequencies nearby the transition range. It is important to remark that for 4.5 kHz (Figure 17.a), the radiation is mainly dominated by the midrange loudspeaker; for 5.8 kHz (Figure 17.b) the system is in the transition range and for 6.1 kHz (Figure 17.c) the tweeter is the principal acoustic source. Finally, for 7.4 kHz (Figure 17.d) the duct modes are evidenced.

It can be appreciated that the system radiation for frequencies bellow 6 kHz can be approximated as a

plane wave prapagated in a duct, since the radius of the mouth of the compressor driver (25.1 mm) is lower than the wavelenght propagating inside of it.

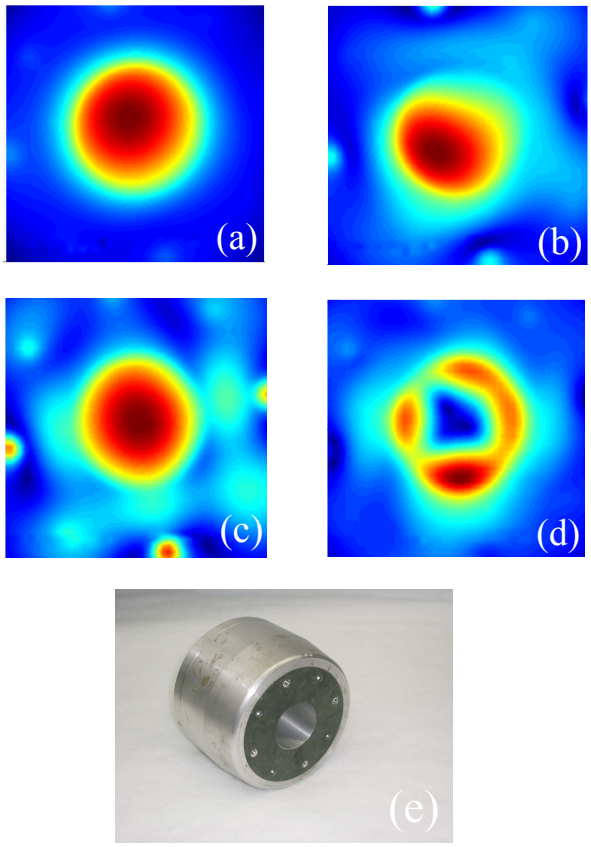


Figure 17: Sound pressure spatial distribution at the hologram plane for different frequencies: (a) 4.5 kHz, (b) 5.8 kHz, (c) 6.1 kHz and (d) 7.4 kHz. (e) Prototype frontal view.

For frequencies above 7 kHz, the propagation in the folded duct does not accomplish this criteria anymore, and hence the internal geometry must be modified to reduce the influence of modal behaviour and to improve the output load impedance matching.

## 5. CONCLUSIONS

In this paper was described the process carried out to adapt a numerical model established in the literature to the study of a coaxial speaker. This model incorporates specific information about the geometry of the radiating system by numerically modeling the load impedance it presents to each loudspeaker.

The model has been contrasted with experimental data and can be a powerful tool to reduce time and costs in the design process and to predict quite closely the frequency response and harmonic distortion of the radiating system considered. It also incorporates a module that allows hearing the effect of the variation of any parameter in order to check, in a first approximation, if small changes in these physical parameters are aurally perceptible.

Besides the experimental and numerical study, an analysis of the interaction between the speakers was performed by applying the NAH technique. The results reveal information about the wave propagation inside the duct, important for the internal geometry optimization and to improve the acoustic impedance coupling.

## 6. REFERENCES

[1] A. Voishvillo, Nonlinearity in Horn Drivers-Where the Distortion Comes From?, 113th AES convention, Los Angeles, Oct 5-8, 2002

[2] W. Klippel, Nonlinear System Models for Horn Loudspeakers, 99th AES convention, New York, Oct 6-9, 1995

[3] H.Schurer, A. Berkhoff, Modeling and Compensation of Nonlinear Distortion in Horn Loudspeakers, 96th AES convention, Amsterdam, Oct 6-9, 1995

[4] A.N. Thiele. Loudspeakers in vented boxes, parts i and ii. Journal of Audio Engineering Society, pp. 19:382-392, 471-483, 1971.

[5] W. Klippel, Assessing Large Signal Performance of Transducers, Klippel GmbH

[6] W. Klippel, Loudspeaker nonlinearities - cause, parameters, symptoms, J. Audio Eng. Soc., vol. 54, pp. 907–939, 2006.

[7] M. Dodd, W. Klippel, and J. Oclee-Brown. Voice coil impedance as a function of frequency and displacement. AES Convention:117th. Audio Engineering Society, October 2004.

[8] M. Piotr, P. Balaz, and B Laback, Multiple Exponential Sweep Method for Fast Measurement

of Head-Related Transfer Functions. J. Audio Eng. Soc., vol. 55, No. 7/8, 2007 July/August.

[9] J.D. Maynard, E.G. Williams, y Y. Lee, "Nearfield acoustic holography: I. Theory of generalized holography and the development of NAH", Journal of the Acoustical Society of America, Vol.78, N_ 4, pp. 1395-1413, (1985).

[10] E.G. Williams y H.D. Dardy, "Nearfield acoustical holography using an underwater, automated scanner", Journal of the Acoustical Society of America, Vol. 78, N_ 2, pp. 789-798, August (1985).

[11] E.G. Williams, "Fourier Acoustics Sound Radiation and Nearfield Acoustical Holography", Ed.Academic Press, (1999).

[12] Williams, "Numerical evaluation of the radiation from unbaffled, finite plates using FFT", Journal of the Acoustical Society of America Vol. 74, July (1983).